SUPPLEMENTAL MATERIAL

Expanded Methods

Patient samples

Ethics committee approval for the use of human material was obtained from the Medical University of Innsbruck (AN2014-026 340/4.34). Informed consent was obtained and valve tissue was then collected from (a) patients undergoing heart valve replacement because of CAVD and (b) patients undergoing heart transplantation (HTX) for reasons other than valvular disease (controls). Tissue was obtained in the operating room under sterile conditions and was placed in sterile M199 culture medium (Life Technologies, Carlsbad, CA) supplemented with 10% fetal calf serum (FCS), penicillin, streptomycin and L-glutamine. Samples were transported to the laboratory on ice and processed immediately on arrival.

Cell isolation and culture

Valvular interstitial cells from patients undergoing aortic valve replacement or heart transplantation were isolated via collagen digestion. Valves were rinsed in EBSS and digested with collagenase (Sigma, St. Louis, MO; 2.5 mg/mL in M199) at 37°C for 30 minutes. The tissue samples were then vortexed and the supernatant, containing endothelial cells, was removed. Collagenase was added to the remaining valve tissue (1 mg/ml), which was then incubated at 37°C for 3 h. For mechanical disintegration, the tissue was vortexed and repeated aspirated in a pipette. The supernatant was transferred to a new tube and subjected to centrifugation (300 x *g* for 8 minutes at 4°C). The cells were resuspended in M199 medium supplemented with 10% fetal calf serum, penicillin, streptomycin, L-glutamine and amphotericin B (2.5 mg/l).

For the ageing experiment, VICs were treated with 8mM Hydroxyurea (Sigma) for 48 h. For ß-galactosidase staining a commercially available kit from Cell Signaling Technology (Danvers, USA) was used according to the manufacturer's protocol.

SV40-immortalized mouse embryonic fibroblasts (MEFs) were cultured in DMEM supplemented with 4.5 g/l glucose (Lonza, Basel, Switzerland), 10% FCS (Sigma, St. Louis, MO), penicillin, streptomycin, L-glutamine and amphotericin B (2.5 mg/l).
Human osteoblasts were purchased (Promocell, Heidelberg, Germany) and cultured in DMEM supplemented with 4.5 g/L glucose (Lonza, Basel, Switzerland), 10% FCS (Sigma, St. Louis, MO), penicillin, streptomycin, L-glutamine and amphotericin B (2.5 mg/l).

WT and TLR3$^{-/-}$ human dermal fibroblasts were kindly provided by Jean-Laurent Casanova and were cultured in DMEM supplemented with 4.5 g/l glucose (Lonza, Basel, Switzerland), 10% FCS (Sigma, St. Louis, MO), penicillin, streptomycin and L-glutamine. Human CTR dermal fibroblasts were provided by the group of Villunger and were cultured in DMEM supplemented with 4.5 g/l glucose (Lonza, Basel, Switzerland), 10% FCS (Sigma, St. Louis, MO), penicillin, streptomycin and L-glutamine.

All cells were cultured under standard conditions (37°C, under an atmosphere containing 5% CO_2). Cells were passaged at 70-90% confluence, and were used only until passage 7, as previously described [21]. Polyinosinic:polycytidylic acid (Poly(I:C); Invivogen, San Diego, CA) was used to stimulate cells at a concentration of 20 µg/ml or 5 µg/ml, depending on the assay. For TLR3 blockade, we used the commercially available dsRNA/TLR3 inhibitor (R)-2-(3-chloro-6-fluorobenzo [b] thiophene-2-carboxamido)-3-phenyl-propanoic acid (Merck, Darmstadt, Germany) at a concentration of 1 µg/ml, as previously described [55]. LY294002 (Invivogen, San Diego, CA), a PI3K inhibitor, was used at a concentration of 10 µM. For IFNAR1 blockade, a specific blocking antibody (Invitrogen, Carlsbad, CA) was used at a concentration of 4 µg/ml.
A stable HEK (human embryonic kidney) reporter cell line (TLR3/ISRE LUCPorter; Imgenex, USA) was purchased for assays on the luminometer. Cells were cultured in accordance with the supplier's protocol, in DMEM supplemented with 4.5 g/l glucose (Lonza, Switzerland),

10% FCS (Sigma, St. Louis, MO), penicillin/streptomycin, 4 mM L-glutamine and 3 mg/ml puromycin (Gibco, USA) as a selection agent.

Reporter experiments were performed as previously described [56]. For studies of protein levels, SF21 cells were purchased from Thermo Fisher Scientific (#11497013) and cultured in Gibco™ Sf-900™.

SFM was supplemented with penicillin, streptomycin and L-glutamine. Stretching was applied with a Flexcell bioreactor (Flexcell International Corporation, Burlington, NC) at a cyclic strain of 15%.

Transfection

The siRNA knockdown was performed with DharmaFECT1 Transfection Reagent (horizon, #T-2005-01). Transfection was performed according to the instructions provided by horizon™. The siRNAs used were purchased from Santa Cruz Biotechnology (**Table S3**).

As a negative control, we used AllStars Neg. Control siRNA (20 nmol) (Qiagen, #1027281) under the same conditions. Crispr/Cas9 protocol (using pLenti-Crispr V2) was used to knockout TLR3 in BJ1 human fibroblast cell line. BJ1 cells were transduced with lentivirus particles containing pLenti-Crispr V2 containing guide RNA sequences, and selected with puromycin to obtain single clones. Sanger sequencing of the single cell clones confirmed a homozygous deletion (V82lFS99*) in TLR3.

Calcification assay

VICs were subjected to a calcification assay for the functional evaluation of osteoblastic activity. Cells were cultured in osteogenic medium containing 10 mmol/l beta-glycerophosphate, 10 nmol/l vitamin D3, and 10 nmol/l dexamethasone, as previously described [10]. The medium was replaced every three days. The supernatant was then analyzed for alkaline phosphatase activity with a commercially available alkaline phosphatase assay kit (Abcam, Cambridge, UK). The cells were carefully rinsed in PBS, fixed by incubation with 4%

paraformaldehyde, washed with distilled water, and Alizarin Red S staining solution (Alfa Aesar, Haverhill, MA) was then added to the fixed cells, which were incubated at room temperature for 20 minutes. Staining was visualized under a Zeiss Axioplan 2 microscope (Zeiss, Oberkochen, Germany). Images were processed with Adobe Photoshop CS5.1 for Mac (Adobe Systems Inc., San Jose, CA, USA) and analyzed with ImageJ software (National Institutes of Health, Bethesda, MA).

RNA sequencing analysis

Total RNA was isolated from five samples (VICs, cultured in calcification media and treated for 72 h with 20 μg/ml Poly(I:C), untreated controls, and human osteoblasts) and subjected to transcriptomic analysis for gene-expression profiling. For the RNA sequencing analysis shown in **Figure 2**, a 2100 Bioanalyzer and RNA 6000 Nano LabChip kits (Agilent Technologies) were used to assess RNA integrity (all RINs>9). We used TruSeq® Stranded mRNA HT technology for library preparation, according to manufacturer's protocol, and Illumina NextSeq® 500 1x75 bp single-end sequencing was performed at IMGM® laboratories (Martinsried, Germany).

Additional RNA sequencing analyses of human VICs (untreated and treated with 20 μg/mL Poly (I:C) for 72 h), human osteoblasts, and human dermal fibroblasts (untreated and treated with 20 μg/mL Poly (I:C) for 72 h) in **Figure S8** were performed in triplicate at Novogene Inc. (UK) on llumina NovaSeq 6000 device (PE150). Reads were mapped to the human reference genome (hg38) using splice aware aligner STAR 2.7.1a. Quantifications on NCBI gene models (hg38refGene) were performed using featureCounts v2.0.0. Differentially expressed genes were identified using DESeq2 and further analyzed accordingly[57].

All primary sequencing analyses were performed with CLC Genomics Workbench (9.5.3), including quality control and mapping onto the human reference genome (GRCh38.p7). Differential expression analyses were performed on raw count data with an exact test based on a negative binomial distribution (edgeR version 3.4.0)[58]. *P*-values were adjusted according to

the Benjamini-Hochberg method based on false discovery rate (FDR). Only genes for which at least four-fold differences in expression were detected were considered. The overrepresentation of gene ontology terms and pathways among differentially expressed genes was assessed with DAVID (6.8)[59] and ConsensusPathDB [60]. Gene set enrichment analysis was performed on log2-fold change preranked data with GSEA software [61] and gene sets for biological hallmark processes and pathways (MSigDB), a calcification signature derived from previous publications, and signatures of differentially expressed genes for calcific aortic valve stenosis versus control[62] (data from GSE12644 reanalyzed with the R package limma [63], including genes with more than two-fold differences in expression and an FDR<0.05). Heat maps were generated with Genesis version 1.8.1[64] for log2-fold change data.

RT-PCR

RT-PCR was performed as previously described [22]. Total RNA was extracted from homogenized tissue or cell lysates with the Total RNA Miniprep Kit (New England BioLabs, Frankfurt, Germany), according to the manufacturer's instructions. PCR was performed in a final volume of 12.5 µl containing 2.5 µl cDNA, 6.25 µl Master Mix, 1 µl of fluorogenic hybridization probe, 10 µM primer and 2.75 µl distilled water. Amplification was performed in a two-step PCR (40 cycles; 15 s of denaturation at 95°C, 1 minute at the annealing temperature and then 30 s at 60°C for extension). Specific gene expression was normalized against the expression of the housekeeping gene, GAPDH, according to the formula $2^{-\Delta Ct}$. Relative gene expression was calculated by the

2-DDCt method. Mean Ct values were calculated from double determinations, with samples being considered negative if Ct values exceeded 40 [22]. Primers were designed with Primer3Plus Software and obtained from Microsynth AG (Balgach, Switzerland). The sequences of the primers used are listed in **Table S4**.

Lysate preparation and immunoblotting

Protein was extracted from tissue or cell lysates was extracted in Radioimmunoprecipitation Assay Lysis Buffer (150 mM NaCl, 1% NP-40, 0.5% sodium deoxycholate, 0.1% SDS and 50 mM Tris (pH 8.0)). For the extraction of nuclear or cytosolic proteins, we used the NE-PER™ Nuclear and Cytoplasmic Extraction Reagents Kit (Thermo Fisher Scientific, #78835).

The proteins were then separated by electrophoresis in SDS-polyacrylamide gels of various percentages and transferred to nitrocellulose membranes, as previously described [65]. The membranes were blocked by incubation with 5% BSA in TBS 0.1% Tween, 5% milk in TBS 0.1 % Tween or StartingBlock™ (TBS) Blocking Buffer (Thermo Fisher Scientific, #37542). They were then incubated with the primary antibodies listed in **Table S5.** Antibodies were tested for their specificity as shown in **Figure S10.**

The membranes were then incubated with the secondary antibody, and chemiluminescence was detected by incubation with either Clarity™ Western ECL Substrate (Bio-Rad, #170-5060) or ECL™ Prime Western Blotting Detection Reagents (Amersham™, #RPN2232).

Histology

Tissue samples were fixed in 4% paraformaldehyde in PBS (0.1 M) and embedded in paraffin. We cut 5 µm tissue sections, which were then stained with a standard hematoxylin and eosin staining protocol (Thermo Fisher Scientific, Waltham, MA). Additional sections were stained with a silver staining kit as described by von Kossa (Merck, Darmstadt, Germany) and with Oil-Red-O (Sigma, St. Louis, MO).

Bone tissue was decalcified by incubation with ethylenediaminetetraacetic acid (EDTA) for three weeks at room temperature before tissue processing. Immunohistochemistry was performed as previously described [66]. Paraffin-embedded sections were subjected to heating in sodium-citrate buffer (10 mM sodium-citrate, 0.05% Tween 20, pH 6.0) for antigen retrieval.

The sections were then blocked by incubation for 30 minutes in 5% serum in PBS. The following primary antibodies were used for staining **(Table S6)**:

Primary antibodies were incubated overnight with the sections at 4°C. Alexa Fluor 568- and Alexa Fluor 488-conjugated IgG antibodies (Life Technologies, Carlsbad, CA) were used as the secondary antibodies, and 40,6-diamidino-2-phenylindole (DAPI; Life Technologies, Carlsbad, CA) was used for nuclear counterstaining. Sections were examined under a Zeiss Axioplan 2 light microscope (Zeiss, Oberkochen, Germany), and immunofluorescence was assessed with a Leica SP5 confocal microscope (Leica, Wetzlar, Germany). Images were analyzed with ImageJ software (National Institutes of Health) and processed with Adobe Photoshop CS5.1 for Mac (Adobe Systems Inc., San Jose, CA, USA).

Mice were anesthetized with 1.5% isoflurane (AbbVie, Vienna, Austria) and 98.5% O_2 and placed on a warming pad at 37.5°C before and during the procedure. We used the Vevo 1100 imaging system and Visual Sonics Software Vevo Lab 1.7.1 (Visual Sonics, Toronto, Canada) for ultrasound examinations. Measurements of the parasternal longitudinal axis (PSLAX) were performed with a MS400 (18-38MHz) transducer. Aortic valve opening diameter and aortic valve leaflet thickness were determined in M-Mode by freehand measurement [67]. Flow measurements were performed with Pulsed Wave Doppler Imaging as described previously [68,69]. Images were acquired from an upper right parasternal view. Pulsed-wave Doppler was used (only PW available in Vevo/Small animal echo), angle correction was performed individually within 60 degrees to capture maximal velocities. Maximal velocities are labeled as peak velocities. All measurements and analyses were performed blinded.

Micro-computed tomography analysis

Hearts were fixed by incubation in 4% formaldehyde for 24 hours, and were then incubated for 24 hours in an iodine-based contrast medium solution (Jopamiro 300 mg; BIPSO, Singen, Germany) before being dried to critical point. Femurs were fixed in 4% formaldehyde after

detachment from the hip joint. Experiments were performed with a VivaCT 40 (Scanco Medical AG, Brüttisellen, Switzerland), using 1000 projections, with 2048 samples and a 21.5 mm field of view (FOV), resulting in an isotropic resolution of 10.5 µm per voxel. The tube settings were a voltage of 45 kV, current of 177 µA current and an integration time of 380 ms per projection. For assessments of the thickness of the aortic wall and the aortic valve leaflets, we used a semi-automatic algorithm. Thickness and morphology was calculated as previously described [70].3D images were generated with the software tool provided by the manufacturer.

Zebrafish model

Fish were maintained and raised under standard pisciculture conditions. VitD3 treatments were administered. Briefly, 15 animals (5 dpf) were pooled per six-well pate and incubated for 5 days at 28°C in 4 ml E3 medium supplemented with 0.1% DMSO and various other compounds, as indicated. Larvae were fixed by overnight incubation in 4% PFA. The final concentrations of the compounds added were 5 µg/ml for the TLR3-inhibitor (Merck, Darmstadt, Germany) and 200 ng/ml for VitD3 (Sigma, St. Louis, MO). Dilutions were generated from stock solutions of 10 mg/ml TLR3-INH and 200 mg/ml VitD3 in DMSO. Solutions containing VitD3 were replaced daily. All experiments were performed in duplicate. Alizarin Red staining was performed according to a slightly modified version of a published procedure [71]. After staining, the larvae were transferred to 100% glycerol and imaged. Area measurements were carried out as described[72].

Whole area: For each larva, three independent ventral view images were taken with a Leica MZ16FA, with standardized stereomicroscope settings. After imaging, the larvae were embedded. Data quantification was performed with ImageJ. Standard white balance was used for background subtraction. Images were converted to grayscale (8 bit) and the threshold was set at 225. The stained area excluding the otoliths was measured. The data points indicate the mean areas on the three images obtained per embryo.

Operculum area: Larvae were imaged laterally, from both sides, under standard microscope settings. Area was measured as described above.

Statistical analysis

Results are presented as the mean ± standard error of the mean. Statistical comparisons between two groups were performed by Student's *t*-tests or Mann-Whitney tests, whereas comparisons between multiple groups were performed by one-way ANOVA with Tukey post hoc analysis for statistical significance. *P*-values < 0.05 were considered statistically significant.

Specific statistical data analyzed in figures

Figure 1f: one-way ANOVA: treatment, treatment $F(2, 22) = 25.06$, $P<0.0001$; Figure 1g: one-way ANOVA: treatment, treatment $F(2, 23) = 14.90$, $P<0.0001$; Figure 1h: one-way ANOVA: treatment, treatment $F(2, 23) = 21.17$, $P<0.0001$; Figure 1j: one-way ANOVA: treatment, treatment $F(2, 19) = 7.624$, $P=0.0037$; Figure 1k: one-way ANOVA: treatment, treatment $F(2, 19) = 3.778$, $P=0.0416$; Figure 1l: one-way ANOVA: treatment, treatment $F(2, 13) = 7.688$, $P=0.0063$; Figure 1n: one-way ANOVA: treatment, treatment $F(2, 26) = 10.43$, $P=0.0005$; Figure 1o: one-way ANOVA: treatment, treatment $F(2, 21) = 5.616$, $P=0.0111$; Figure 1p: one-way ANOVA: treatment, treatment $F(2, 23) = 4.794$, $P=0.0182$

Figure 2c: one-way ANOVA: treatment, treatment $F(5, 30) = 261.4$, $P<0.0001$; Figure 2d: one-way ANOVA: treatment, treatment $F(5, 30) = 21.75$, $P<0.0001$; Figure 2i: one-way ANOVA: treatment, treatment $F(2, 41) = 76.91$, $P<0.0001$; Figure 2j: one-way ANOVA: treatment, treatment $F(2, 14) = 13.34$, $P=0.0006$; Figure 2l: one-way ANOVA: treatment, treatment $F(2, 43) = 23.50$, $P<0.0001$; Figure 2m: one-way ANOVA: treatment, treatment $F(2, 15) = 10.61$, $P=0.0013$

Figure 4b: one-way ANOVA: treatment, treatment $F(4, 23) = 1336$, $P<0.0001$; Figure 4c: one-way ANOVA: treatment, treatment $F(5, 34) = 276.7$, $P<0.0001$; Figure 4j: one-way ANOVA: treatment, treatment $F(2, 15) = 6.425$, $P=0.0096$

Figure 5a: one-way ANOVA: WT treatment F(2, 15) = 66.51, P<0.0001, TLR3-/- treatment F(2, 15) = 1.982, P=0.1723, CTR treatment F(2, 15) = 15.10, P=0.0003; Figure 5b: one-way ANOVA: WT treatment F(2, 15) = 7.913, P=0.0045, TLR3-/- treatment F(2, 15) = 1.982, P=0.1723, CTR treatment F(2, 11) = 5.347, P=0.0239; Figure 5e: one-way ANOVA: treatment, treatment F(3, 24) = 2.493, P=0.0843; Figure 5g: one-way ANOVA: treatment, treatment F(3, 22) = 4.119, P=0.0184; Figure 5h: one-way ANOVA: treatment, treatment F(3, 23) = 6.714, P=0.0020; Figure 5j: one-way ANOVA: treatment, treatment F(3, 24) = 7.953, P=0.0007; Figure 5k: one-way ANOVA: treatment, treatment F(3, 22) = 9.846, P=0.0003; Figure 5l: one-way ANOVA: treatment, treatment F(3, 21) = 6.005, P=0.0040; Figure 5m: one-way ANOVA: treatment, treatment F(3, 21) = 9.452, P=0.0004

Figure S1f: one-way ANOVA: treatment, treatment F(2, 15) = 6.152, P=0.0112; Figure S1h: one-way ANOVA: treatment, treatment F(2, 15) = 2076, P<0.0001

Figure S7d: one-way ANOVA: treatment, treatment F(2, 31) = 85.23, P<0.0001

Figure S9b: one-way ANOVA: treatment, treatment F(2, 18) = 13.44, P=0.0003; Figure S9c: one-way ANOVA: treatment, treatment F(2, 18) = 19.47, P<0.0001

Structure analysis and modeling

We selected a docking protocol in which the non-glycosylated proteins were first docked on the basis of shape complementarity[73] or in which docked pre-aligned models based on symmetry considerations were used, with local refinement of the docked models[42]. Docking results were then cross-validated by adding glycans at all consensus sites, ensuring that the docked complex allowed for the presence of the N-linked glycan chains. The plausibility of the model was then assessed in light of known biological data.

huTLR3-ECD

The experimental high-resolution model of the structure of the TLR3 receptor ectodomain (ECD), PDB entry 1ziw[74], was used as a template for modeling a glycosylated and completed

human TLR3-ECD dimer model. All 15 experimentally verified glycosylation sites from 1ziw [75], 2a0z [76], and 5gs0 [77] were decorated with the first eight carbohydrate core units ($GlucNac_2(Fuc)Man_5$) of human glycans in idealized geometry, with the glyca- building tools in *COOT* [78]. Flexible glycan decorations are present *in vivo* and are often only partially visible in the electron density of X-ray structures, but they must be included in the model because they occupy space and may limit possible orientations [79]. Loop 336-343, which is missing from 1ziw, was completed based on data for the humanized mouse TLR3 model 3ciy [75]. All TLR3 structures included identical crystallographic or non-crystallographic dimers, indicating probable binding of the TLR3 receptor to biglycan as a dimer.

BGN

The experimental model of the structure of the glycoprotein core of BGN, PDB entry 2ft3 [41], was used as a template for modeling huBGN. BGN is an obligate biological dimer displaying 98% sequence identity for the mature protein. The 2ft3 structure includes one partially modeled glycan and starts at residue 24 of the mature peptide. The N-terminal O-linked glycosaminoglycan decorations were removed by digestion with chondroitin ABC lyase and are thus absent from the crystal structure model. We performed the following steps to generate a huBGN model for docking: (i) humanization of the sequence with local minimization of the structure in *ICMPro* [43], and (ii) addition of the first residues of a human glycan ($GlucNag_2(Fuc)Man_5$) in idealized geometry to glycosylation sites N234 and N275 with *COOT*[78], in order to assess regions to the regions to be excluded from docking. No attempt was made to model the N-terminal glycosaminoglycan chains because they are not in the vicinity of predicted binding sites.

Binding-site prediction

Binding-site predictions based on the optimal docking areas (ODA) method [80] identified the C-terminus of biglycan as the most likely interaction area **(Fig. 4D)**, consistent with the absence

from the structure models of the N-terminal residues bearing the glycosaminoglycan decorations thought unlikely to be involved in direct protein-protein contacts **(Fig.S6A)**. The BGN glycosylations are distal to the proposed binding region, and are unlikely to hinder the formation of protein-protein contacts.

Possible modes of binding

Both TLR3 and BGN form obligate dimers, and this strongly suggests that they also interact as dimers *in vivo,* forming either a $(TLR3_2)(BC_2)$ complex between the respective dimers (binding mode A) or a $(TLR3_2)(BC_2)_2$ complex (mode B) in which one biglycan dimer binds to each of the subunits of the TLR3 dimer. Mode A requires the maintenance of the collinearity of the dimer axes, effectively reducing the docking search space. The Euler axis for each dimer was computed from the directional cosine matrix obtained by superimposing the models in *COOT*[78], its location being calculated as half the superimposition translation vector. The two dimer axes were then superimposed with *COOT,* providing pre-aligned starting models for subsequent protein-protein docking and refinement in the *Rosetta* module *Docking2*[42]. The biological evidence is not in favor of binding mode B, because this model would probably result in uncontrolled multimerization between many TLR3-ECDs or steric clashes with BGN and the endosome membrane.

Validation of the model

The docking models in mode A with high scores were consistent with the posterior predictions of the optimal docking areas method [80]. Discrimination of the tightly clustered optimized dimer models in mode A was based on interface analysis, with selection of the model with the largest interface area and a negative interface formation energy (ΔG_i).

The most probable and compelling complex model complies with multiple structural and biological restraints and provides a plausible approximation of the most likely mode of binding

between huTLR3 and huBGN. It is not yet known whether huBGN binds to hTLR3 in a chondroitinated (huBGN^{+}) or unchondroitinated form *in vivo*. *In vitro* core protein interactions of the huBGN C-terminal region are sufficient for interaction with TLR3-ECD, and the model also allows for the possibility of huBGN^{+} binding, because there is sufficient space accessible to accommodate exposed N-terminally located glycosaminoglycan decorations absent from the crystal structure templates. There is also sufficient space to accommodate the complex glycans without steric interference between the binding partners. After glycan torsion adjustment, the model was refined with the *refineInterface* module of ICMPro.

Protein interface analysis [81] indicated the presence of a buried surface between the complex dimers of about 800 Å^2 in area, with an interface energy of -2.4 kcal. The interface parameters of the obligate hBGN dimer were calculated simultaneously by cross-validation (~1300 Å^2 buried surface with -2.0 kcal interface energy). The data for the buried complex interface indicate a weaker interaction than expected for an obligate dimer such as huBGN, but significantly stronger than would be expected for a crystal contact [82]. A weak but plausible interaction between huTLR3 and huBGN is consistent with the weak binding interaction observed in the SEC experiments.

The role of the 336-343 loop of TLR3 proximal to the binding site remains unresolved. This loop is cleaved at an unknown position *in vivo* [83] and it is unknown whether any residues are lost in the process. No attempt was made to predict possible additional binding contacts between this hTLR3-ECD loop and hBGN, but the model includes sufficient space to accommodate the loop residues should such an interaction occur.

Production of recombinant TLR3 ECD

The human TLR3-ECD (27-700) was modified with an N-terminal gb67 leader and a C-terminal 6x poly-histidine tag and the sequence was produced synthetically (Geneart) and

inserted into a pFastBac1 vector. A baculovirus carrying this vector was generated and underwent large-scale amplification in an Sf21 insect cell-line (Bac-to-Bac®). One liter of Sf21 cell culture was infected and harvested at 72 hours. The culture was centrifuged at 1000 × *g* for 30 min and the supernatant was filtered through a nitrocellulose membrane with 0.2 µm pores. The filtrate was loaded onto a 5 ml His Trap EXCEL column (GE, 17-3712-06) with a peristaltic pump. The column was washed with 10 column volumes (CV) of buffer (20 mM HEPES pH 7.5, 150 mM NaCl) and protein fractions were eluted with 20 mM HEPES pH 7.5, 150 mM NaCl and 500 mM imidazole. The protein fractions were analyzed by SDS-PAGE and TLR3-containing fractions were pooled and concentrated to a final volume of ~500 µl with a spin concentrator (Vivaspin®20) with a 10 kDa molecular weight cutoff. TLR3 was subjected to size exclusion chromatography (SEC) on a Supedex200 Increase 10/300 GL column (GE, 28990944) equilibrated with 150 mM NaCl, 20 mM HEPES, pH 7.5. TLR3-containing fractions were analyzed by SDS-PAGE, pooled and concentrated to 1 mg/ml. Protein concentration was estimated by measuring absorbance at 280 nm (MW= 77.4 g mol^{-1}, ε=61.9 $mol^{-1}cm^{-1}$) on a Nanodrop spectrometer.

Production of recombinant hBGN

The human BGN (38-368) was modified with an N-terminal Secrecon tag followed by a 6x poly-histidine tag and a Strep-Tag II. The sequence was produced synthetically (Geneart) and inserted into a pFastBac 1 vector. The corresponding virus was generated and subjected to a large scale in an Sf21 insect cell-line (Bac-to-Bac). One liter of Sf21 cell culture was infected ~ at an MOI of about 1 cell/ml and harvested at 72 hours. The culture was centrifuged at 1000 x *g* for 30 min and the supernatant (SN) was filtered through a nitrocellulose membrane with 0.2 µm pores. The SN concentration was adjusted to 20 mM HEPES pH 7.5, 150 mM NaCl and 5 mM imidazole and was degassed before loading onto a 5 ml His Trap EXCEL column (GE, 17-3712-06) with a peristaltic pump. The column was washed with 10 column volumes (CV) of buffer (20 mM HEPES pH 7.5, 150 mM NaCl, 5 mM imidazole) and protein fractions

were eluted with 20 mM HEPES pH 7.5, 150 mM NaCl, 10% glycerol and 500 mM imidazole. The protein fractions were analyzed by SDS–PAGE and BGN-containing fractions were pooled and concentrated to a final volume of ~500 µl with a spin concentrator (Vivaspin®20) with a 10 kDa molecular weight cutoff. The protein was dialyzed for 30 min against 20 mM HEPES pH 7.5 and 150 mM NaCl (Pur-A-Lyzer™ Maxi 6000). The purity of the protein was analyzed by SDS-PAGE and its concentration was estimated by determining absorbance at 280 nm on a Nanodrop spectrometer.

***In vitro* binding experiments based on size exclusion chromatography**

We obtained the core protein of bovine biglycan, by incubating purchased biglycan (Sigma, St. Louis, MO) with chondroitinase ABC (Merck, Darmstadt, Germany) at 37°C for 2 h. The digestion of chondroitin sulfate was verified by electrophoresis and staining with Coomassie Brilliant Blue.

We mixed 185 µl digested BGN (0.5 mg/ml) with 15 µl of TLR3 (1 mg/ml) on ice and incubated the mixture for 30 minutes. The sample was subjected to size exclusion chromatography (Supedex200 Increase 10/300 GL column) with 20 mM HEPES pH 7.5, 100 mM NaCl as the running buffer. Fractions were collected and analyzed by immunoblotting, as described above.

***In vitro* binding experiments based on co-immunoprecipitation**

Equal amounts of the two proteins (TLR3 and BGN) were subjected to co-immunoprecipitation with a monoclonal rabbit anti-human BGN antibody directed against human BGN aa 260-368 (Invitrogen, JB71-31). The coprecipitated proteins were washed with CHAPS buffer (30 mM HEPES pH 7.5, 150 mM NaCl, 1 % CHAPS), subjected to SDS-PAGE and then blotted onto a nitrocellulose membrane (Amersham™ Protran™ Premium, 0.45 µm NC). These membranes were then probed with either an antibody against human TLR3 (Cell Signaling, D10F10) or an antibody against human BGN (R&D Systems, AF2667). Chemiluminescence was assessed with the Clarity™ Western ECL Substrate (Bio-Rad).

Genetic associations with aortic stenosis in humans

The genotypes for GERA were produced by custom designed arrays based on the Affymetrix Axiom Genotyping Solution and this has been previously described [84,85]. Samples were imputed using the HRC reference on the Michigan Imputation Server (https://imputationserver.sph.umich.edu/index.html). Prior to imputation, quality control thresholds (hwe p-value 0.00001, geno 0.03, and mind 0.03) were implemented using plink[86].

The genotyping and imputation of the UK Biobank samples has been previously described[88]. Briefly, genotypes for 488,377 participants were assayed using two similar genotyping arrays. 49,950 participants were genotyped using the UK BiLEVE Axiom Array by Affymetrix (Thermo Fisher Scientific), while 438,427 participants were genotyped using the UK Biobank Axiom Array that shares 95% of marker content with the UK BiLEVE Axiom Array. Markers present on both UKBiLEVE and UKBiobank axiom arrays with maf > 0.0001 and missing rate < 5% were used for pre-phasing. Sample considered outliers for heterozygosity or missing rate were removed prior to phasing. The resulting 670,739 autosomal markers in 487,442 samples were phased using SHAPEIT3[89] with the 1000 Genomes phase 3 dataset as a reference panel [90]. A first imputation was performed using the Haplotype Reference Consortium reference panel[91]. A second imputation with the IMPUTE4 program (https://jmarchini.org/software/) using the merged UK10K and 1000 Genomes phase 3 reference panels was carried out[92]. The two imputed datasets then were combined as previously described[88].

We performed inverse-variance weighted fixed effects meta-analysis in the GERA and UK Biobank cohorts for 6,041 well-imputed (info score ≥ 0.3) variants (minor allele frequency ≥ 0.001) within 50 kb of the *JAK1*, *TLR3*, *IFNB1*, *IFNA1, XYLT1*, *STAT3*, *XYLT2*, or *IFNAR1* transcription boundaries. Cohort-specific estimates for each variant were estimated in separate logistic regression models adjusted for age, age squared, and sex in the GERA cohort, and additionally adjusted for 20 principal components in the UKB.

To assess whether genetically-elevated *XYLT1* expression was causally associated with aortic stenosis, we extracted variants that were common (minor allele frequency ≥ 0.01) with non-ambiguous alleles and $p \leq 1 \times 10^{-3}$ for *XYLT1* expression in the aorta (used as a proxy for the aortic valve, for which tissue was not available) from the Genotype-Tissue Expression (GTEx) Project Version 7 [93]. After removal of variants in high linkage disequilibrium ($r^2 \geq 0.9$), we performed Mendelian randomization using the remaining six variants**,** accounting for linkage disequilibrium between variants (MendelianRandomization R package version 0.4.2)[94]. In a sensitivity analysis allowing for pleiotropy, we applied the penalized weighted median approach.

To better characterize *XYLT1*, we extracted from the PhenoScanner V2 database associations [94] with epigenetic modification reported in a European or mixed population for blood-derived cell types. We queried for all six variants in the genetic instrument for *XYLT1* expression in the aorta as well as variants at $r^2 \geq 0.9$ in a European population (retrieved April 30, 2020).

As a proxy for progression to severe aortic stenosis, we modelled the association of the six *XYLT1* variants with aortic valve replacement among aortic stenosis cases in the GERA (n = 3,469 [397 with valve replacement]) and UK Biobank (n = 2,217 [1,107 with valve replacement]) cohorts, using the same covariate adjustments as described above. For each variant, we meta-analyzed the estimates from the two cohorts using an inverse variance-weighted fixed effects meta-analysis. We then performed Mendelian randomization to assess whether genetically-elevated *XYLT1* expression contributed causally to progression to aortic valve replacement. We applied a more stringent pruning of variants in linkage disequilibrium ($r^2 \leq 0.6$ rather than $r^2 \leq 0.9$; see **Table 3**), yielding a genetic instrument for *XYLT1* expression composed of rs6416675, rs12924407, and rs8054100 (**Table 4**). As a sensitivity analysis to allow for pleiotropy in the instrument, we employed the penalized weighted median method.

Availability of data and materials

All high-throughput data are available via GEO. Accession numbers are GSE138360 and GSE223543. The datasets generated and/or analyzed during this study are available from the corresponding author on reasonable request except for GERA and UK Biobank data, which are available directly from those cohorts upon application.

Supplemental Figures

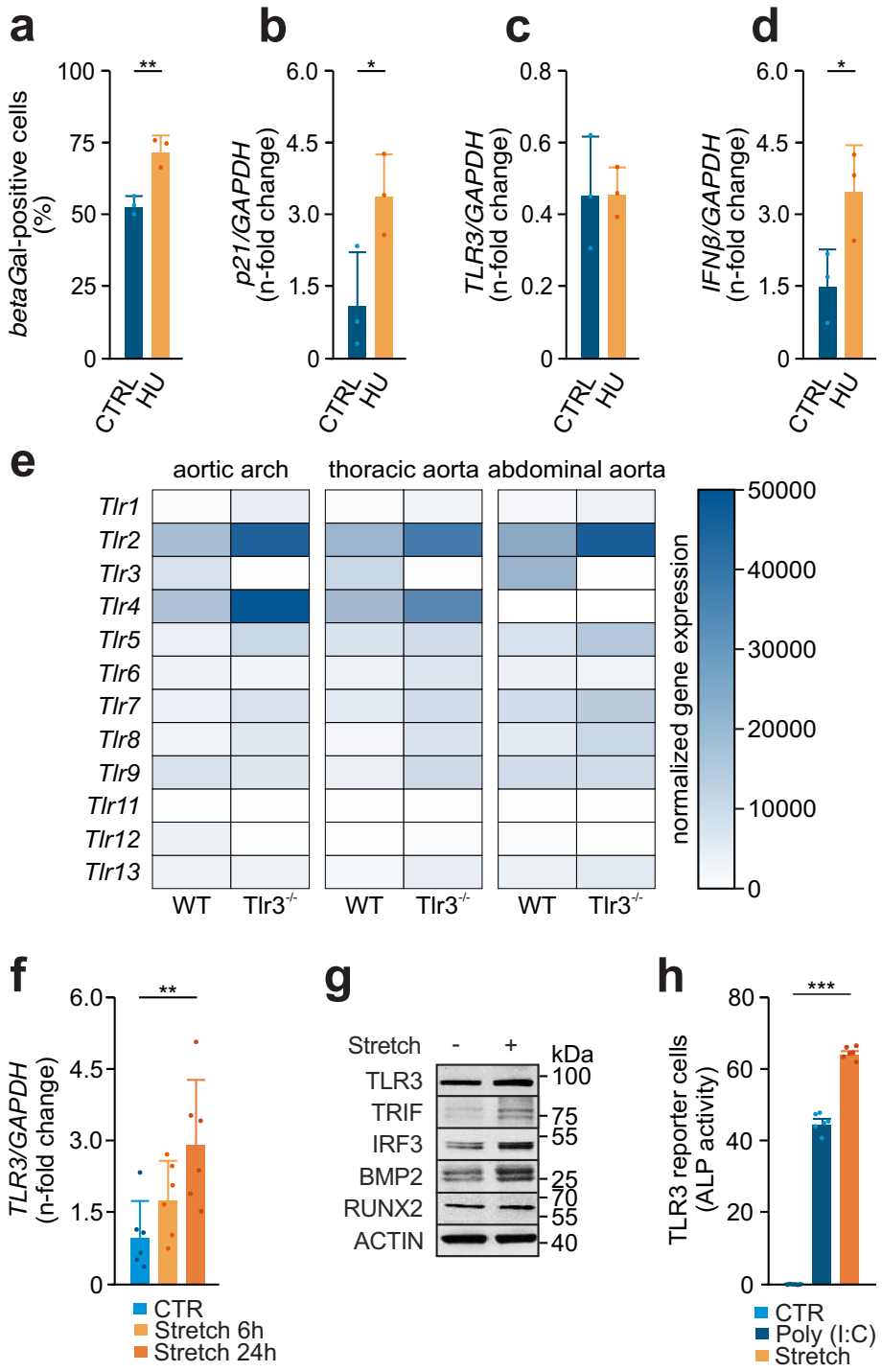

Figure S1: Regulation of Tlr3 and osteoblastic gene expression by mechanical strain.

(a) beta-Galactosidase positive valvular interstitial cells after treatment with hydroxyurea (HU); *n*=3 per group.

(b-d) Gene expression levels of p21, TLR3 and IFN-β, assessed by RT-PCR, in valvular interstitial cells treated with hydroxyurea (HU); *n*=3 per group.

(e) Analysis of gene expression levels of Toll like receptors in murine ascending aortas, descending aortas and abdominal aortas.(mean expression level, *n*=3).

(f) Human VICs subjected to stretch (15%) for 6h or 24h followed by RT-PCR analysis for TLR3 (*n*=6).

(g) Human VICs subjected to stretch (15%) for 6h or 24h followed by immunoblot analysis for TLR3, TRIF, IRF3, BMP2, RUNX2 (Actin served as loading control; *n*=2 independent western blot experiments, representative western blot shown).

(h) HEK293 hTLR3 reporter cells treated with supernatant from stretched VICs or control cells, Poly(I:C) treatment (20 μg/mL) served as positive control (*n*=6).

(a,b,d) Data are presented as mean ± SEM. Two-tailed unpaired *t*-test: *P<0.05, **P<0.01.

(f,h) Data are presented as mean ± SEM. One-way ANOVA with Tukey post hoc test: **P<0.01, ***P<0.001.

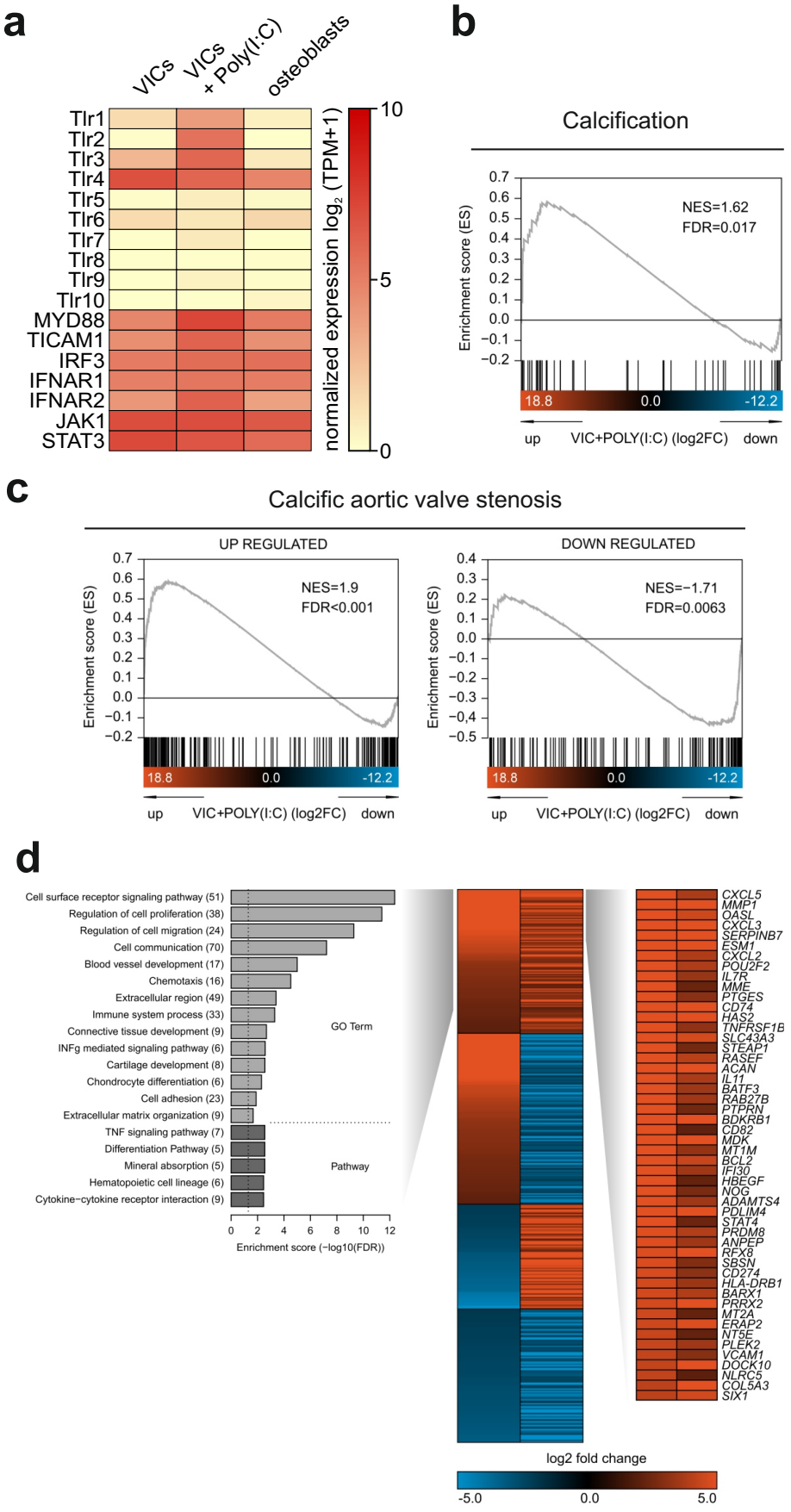

Figure S2: TLR3 activation causes osteoblastic gene expression.

(a) Expression profiles of Toll like receptors and downstream pathway genes in human VICs with or without Poly(I:C) treatment (20 µg/mL) for 72h and human osteoblasts.

(b) Human VICs subjected to stretch (15%) for 6h or 24h followed by immunoblot analysis for TLR3, TRIF, IRF3, BMP2, RUNX2 (Actin served as loading control; *n*=2 independent western blot experiments, representative western blot shown).
(c) HEK293 hTLR3 reporter cells treated with supernatant from stretched VICs or control cells, Poly(I:C) treatment (20 μg/mL) served as positive control (*n*=6).
(b) Gene enrichment set analysis of VICs treated with Poly(I:C) (20 μg/mL) for 72h evaluating regulation of genes involved in calcification or **(c)** in CAVD.
(d) Numbers and expression profiles of at least four-fold change differentially expressed genes in human VICs with or without Poly(I:C) treatment (20 μg/mL) for 72h and human osteoblasts. Significantly over-represented gene ontology terms and pathways among the commonly upregulated genes were indicated. red = upregulated, blue = downregulated, black = not regulated.
(a,c) Data are presented as mean ± SEM. One-way ANOVA with Tukey post hoc test: **P<0.01, ***P<0.001.

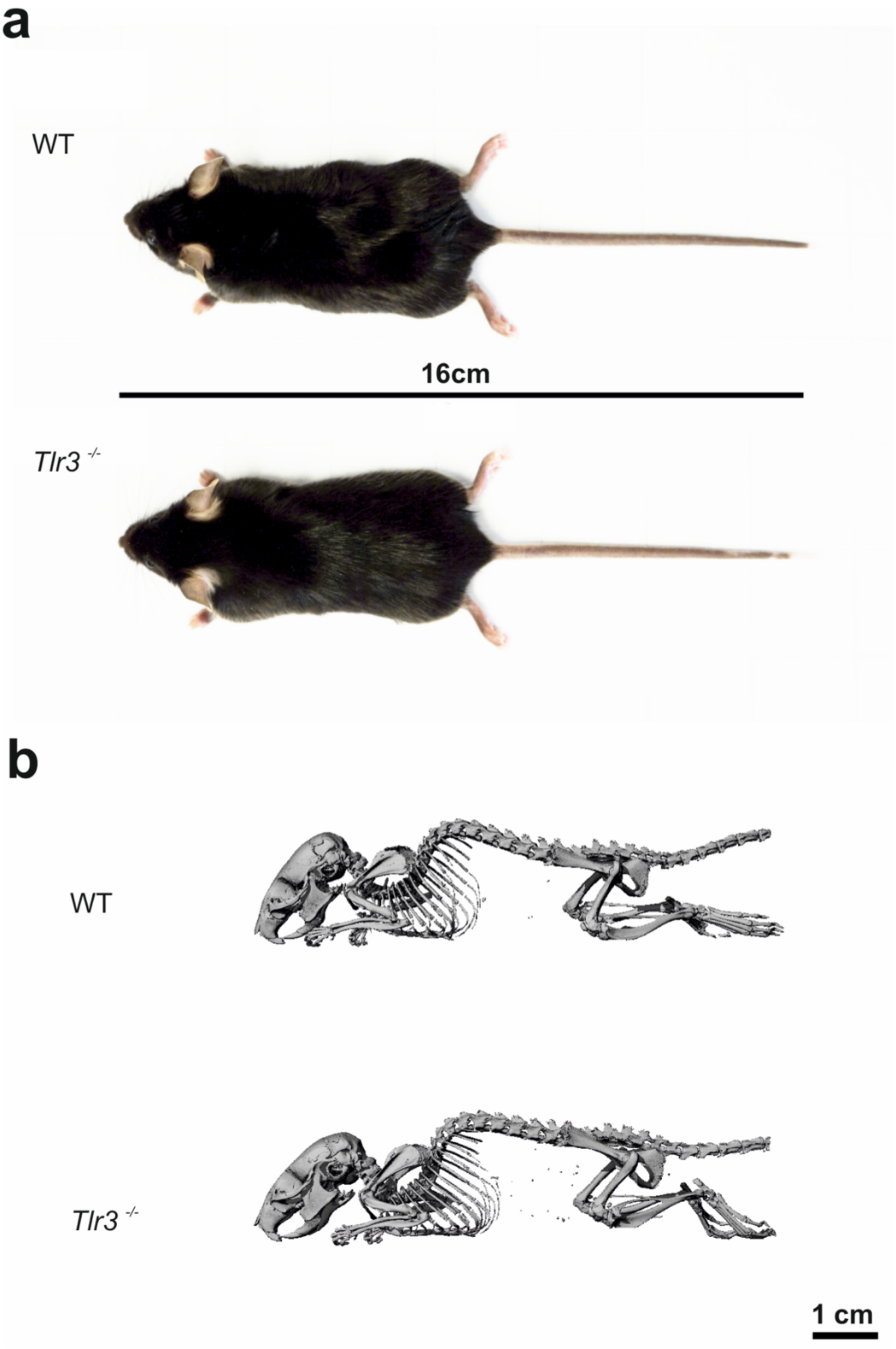

Figure S3: *Tlr3*$^{-/-}$ show no obvious musculoskeletal phenotype.

(a) WT and *Tlr3*$^{-/-}$ showed no obvious difference in size or

(b) skeletal development evaluated via micro-CT scanning.

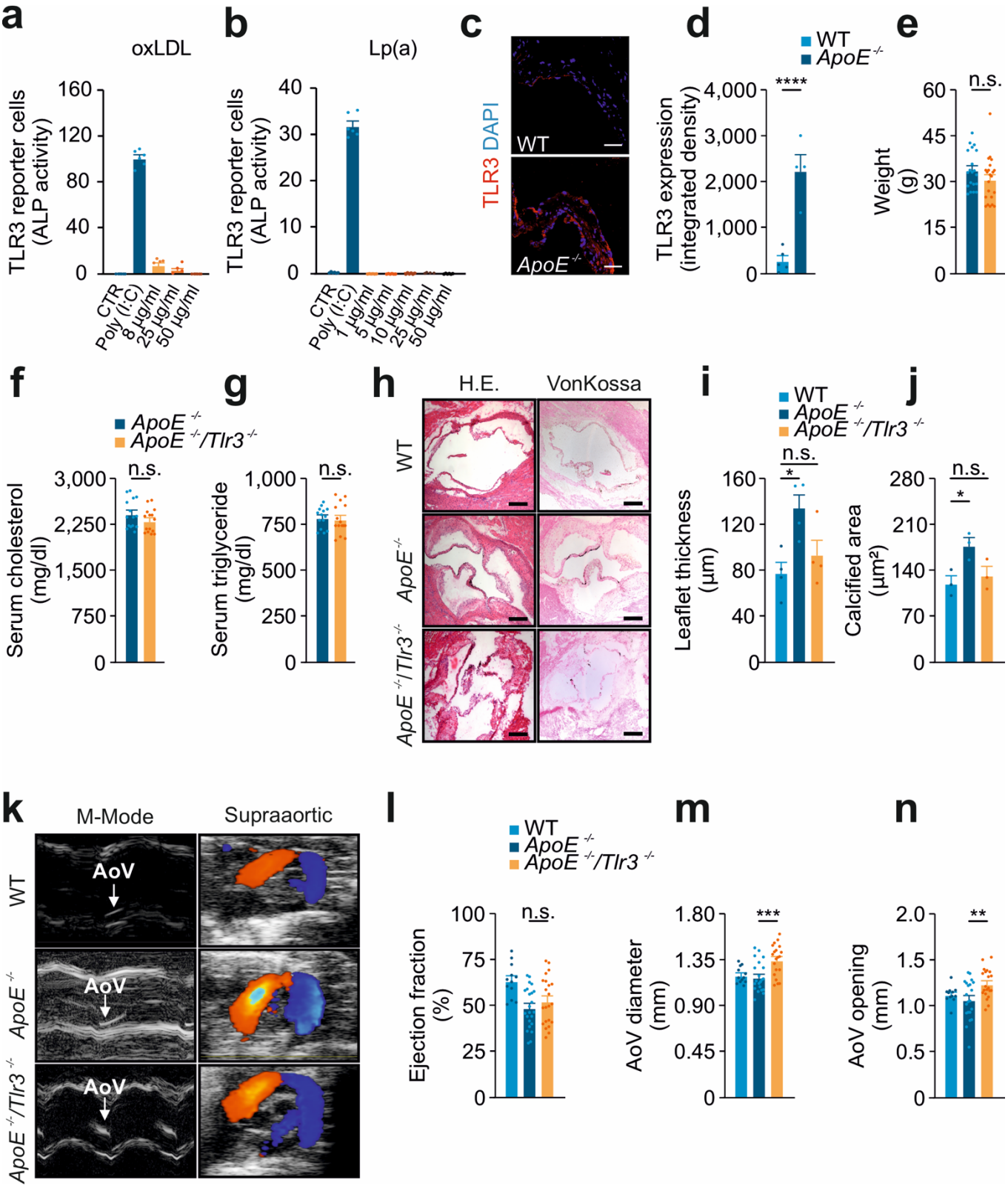

Figure S4: *Tlr3*-deficiency protects mice from hyperlipidemia-induced CAVD.

(a) HEK293 hTLR3 reporter cells treated with Poly(I:C) (20 µg/ml) and oxLDL (*n*=6).

(b) HEK293 hTLR3 reporter cells treated with Poly(I:C) (20 µg/ml) and Lp(a) (*n*=6).

(c) Aortic valves from 12-week-old wild-type mice and *ApoE*$^{-/-}$ mice fed a HFD for 3 months, stained for TLR3 (red: TLR3, blue: DAPI; scale=40 µm) and:

(d) Quantification of TLR3 expression in murine aortic valves (*n*=4-5).

(e) 12-week-old *ApoE*$^{-/-}$ knockout and *ApoE*$^{-/-}$/*Tlr3*$^{-/-}$ double knockout mice fed a HFD for 3 months and subjected to serum cholesterol determinations (*n*=8),
(f) Serum triglyceride determinations (*n*=8) and
(g) Weighing (*n*=22-23).
(h) Aortic valves of 12-week-old wild-type, *ApoE*$^{-/-}$ knockout and *ApoE*$^{-/-}$/*Tlr3*$^{-/-}$ double knockout mice fed a HFD for 3 months and subjected to morphological analysis (scale=250 µm).
(i) Murine aortic valves analyzed for leaflet thickness on H.E. staining (*n*=4 animals per group).
(j) Calcified area of murine aortic valves measured by von Kossa staining (scale=250 µm; *n*=3 animals per group).
(k) Aortic valves of 12-week-old wild-type, *ApoE*$^{-/-}$ and *ApoE*$^{-/-}$/*Tlr3*$^{-/-}$ double knockout mice fed a HFD for 3 months and subjected to hemodynamic analysis via transthoracic echocardiography assessing:
(l) Ejection Fraction (*n*=11-23)
(m) Aortic valve diameter (*n*=12-23)
(n) Aortic valve opening (*n*=12-23).
Data are presented as mean ± SEM. Statistical comparisons: **(d,e,f,g)** two-tailed unpaired *t*-test, ****P<0.0001. **(i,j,l,m,n)** One-way ANOVA with Tukey post hoc tests: n.s. = non-significant, *P<0.05, **P<0.01, ***P<0.001.

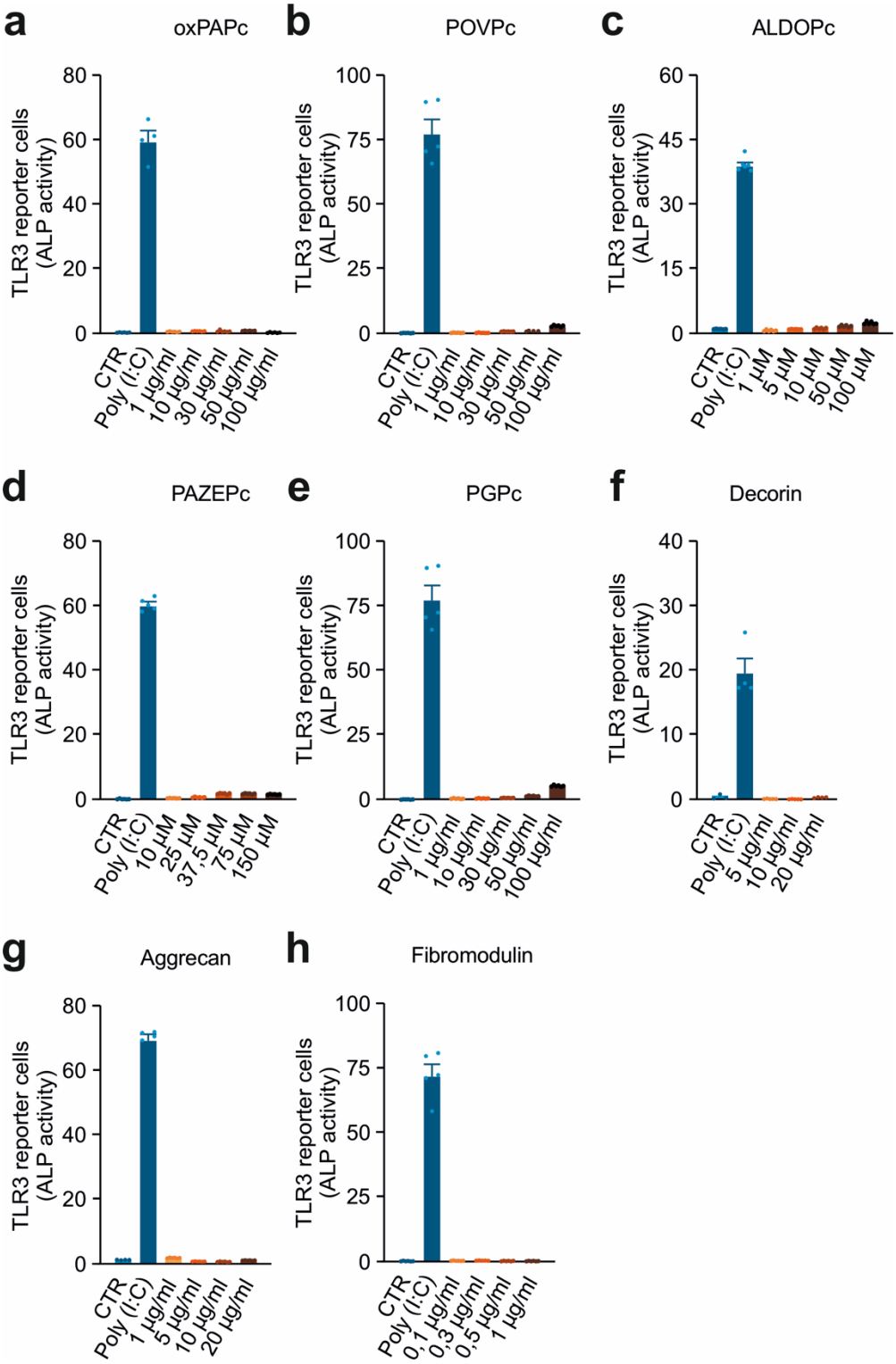

Figure S5: Reporter assays for ligand identification

HEK293 hTLR3 reporter cells treated with Poly(I:C) (20 µg/ml) and the putative TLR3 ligands **(a)** oxPAPC, **(b)** POVPc, **(c)** ALDOPc, **(d)** PAEZEPc, **(e)** PGPc, **(f)** decorin, **(g)** aggrecan, and **(h)** fibromodulin, at various concentrations, for 24 h (*n*=6). All data are presented as the mean ± SEM.

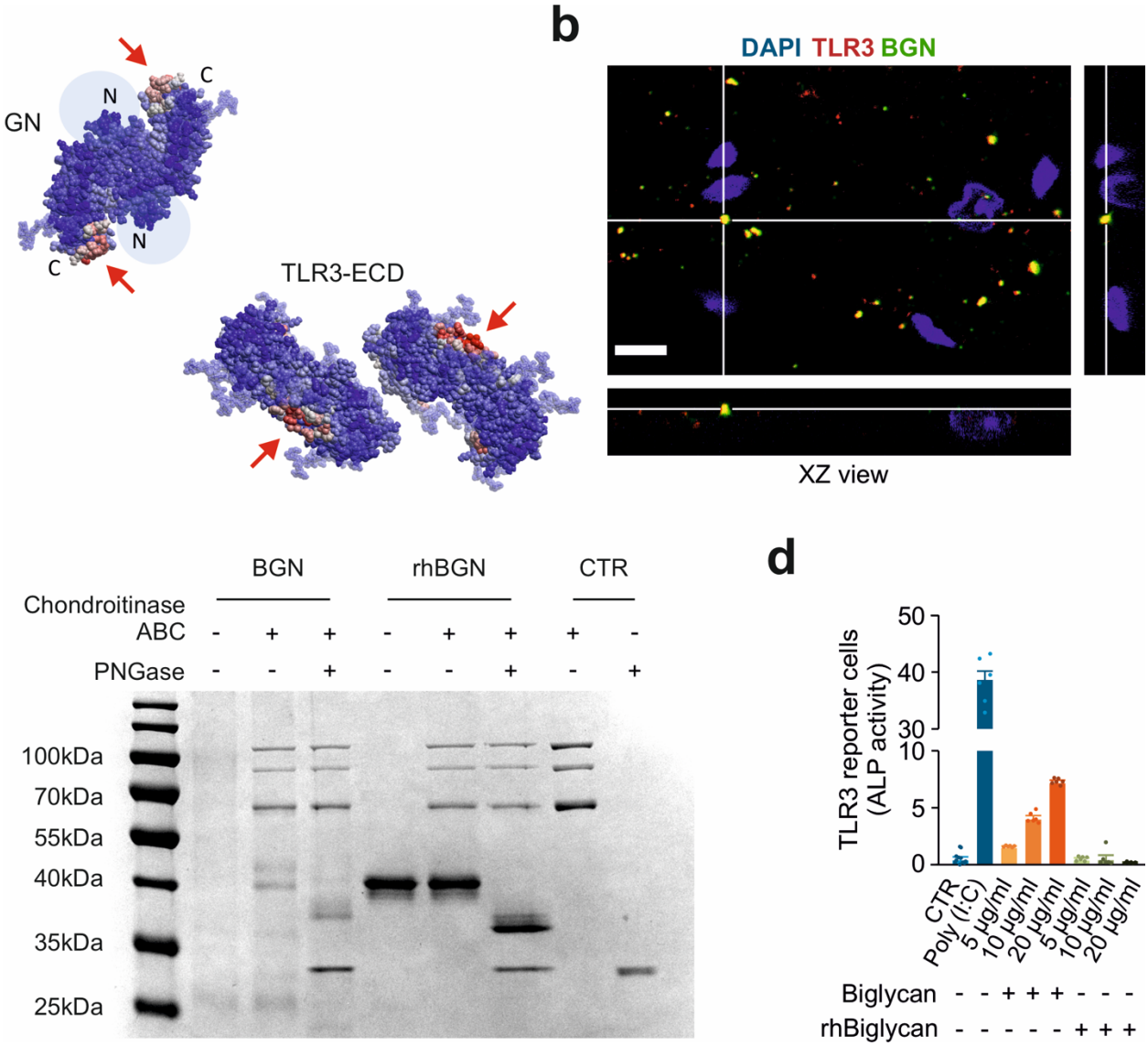

Figure S6: BGN characterization, *silico* modeling of BGN and TLR3 and *Xylt1* variants

(a) Prediction of potential binding regions on BGN and TLR3-Ectodomain (TLR3-ECD) by the ODA method, indicated by the red arrows in the CPK model. The blue spheres indicate the expected sites of N-terminal chondroitin sulfate modifications on BGN.

(b) Co-localization of BGN and TLR3 in murine aortic valves showed by immunofluorescence staining in confocal microscopy (scale bar=5µm).

(c) Comparison of BGN and recombinant rhBGN treated with chondroitinase ABC and PNGase, analyzed by SDS-PAGE with Coomassie Brilliant Blue staining.

(d) HEK293 hTLR3 reporter cells treated with full-length biglycan or biglycan core protein (rh) (*n*=6).

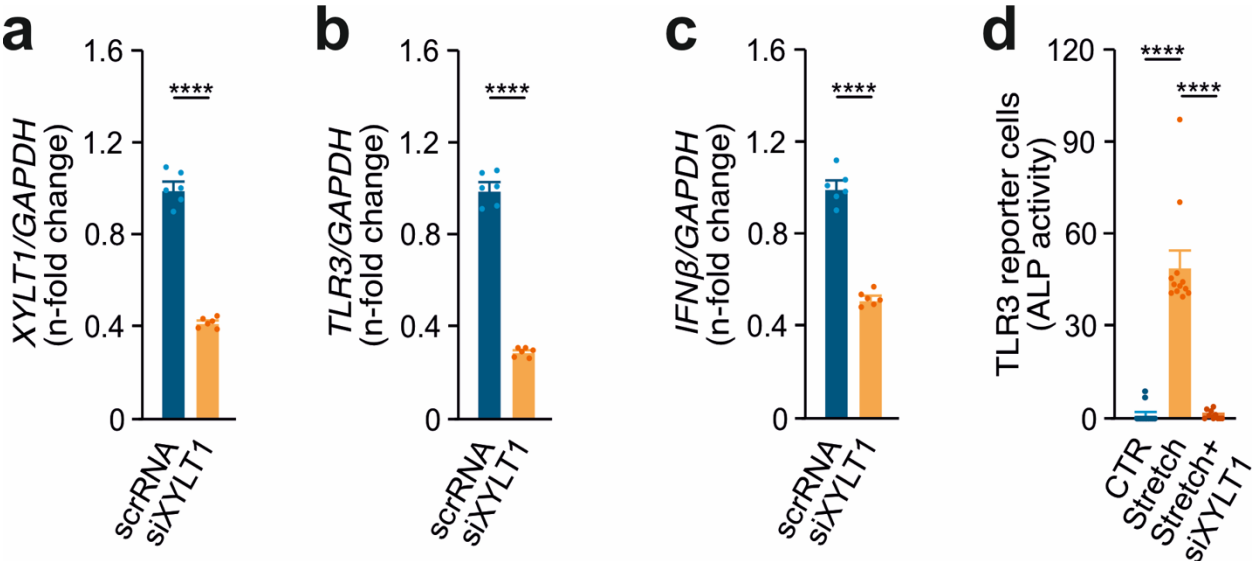

Figure S7: XYLT1-dependent maturation of BGN is required for TLR3 activation

(a) Human VICs transfected with XYLT siRNA or scr RNA for 24 h analyzed by RT-PCR analysis for XYLT1,**(b)** TLR3 and **(c)** IFNß (*n*=6).

(d) HEK293 hTLR3 reporter cells subjected to stretching after XYLT1 knockdown (*n*=6).

All data are presented as the mean ± SEM. Statistical comparisons: **(a),(b),(c)** two-tailed unpaired *t*-tests, ****P<0.0001. **(d)** One-way ANOVA with Tukey post hoc tests: ****P<0.0001.

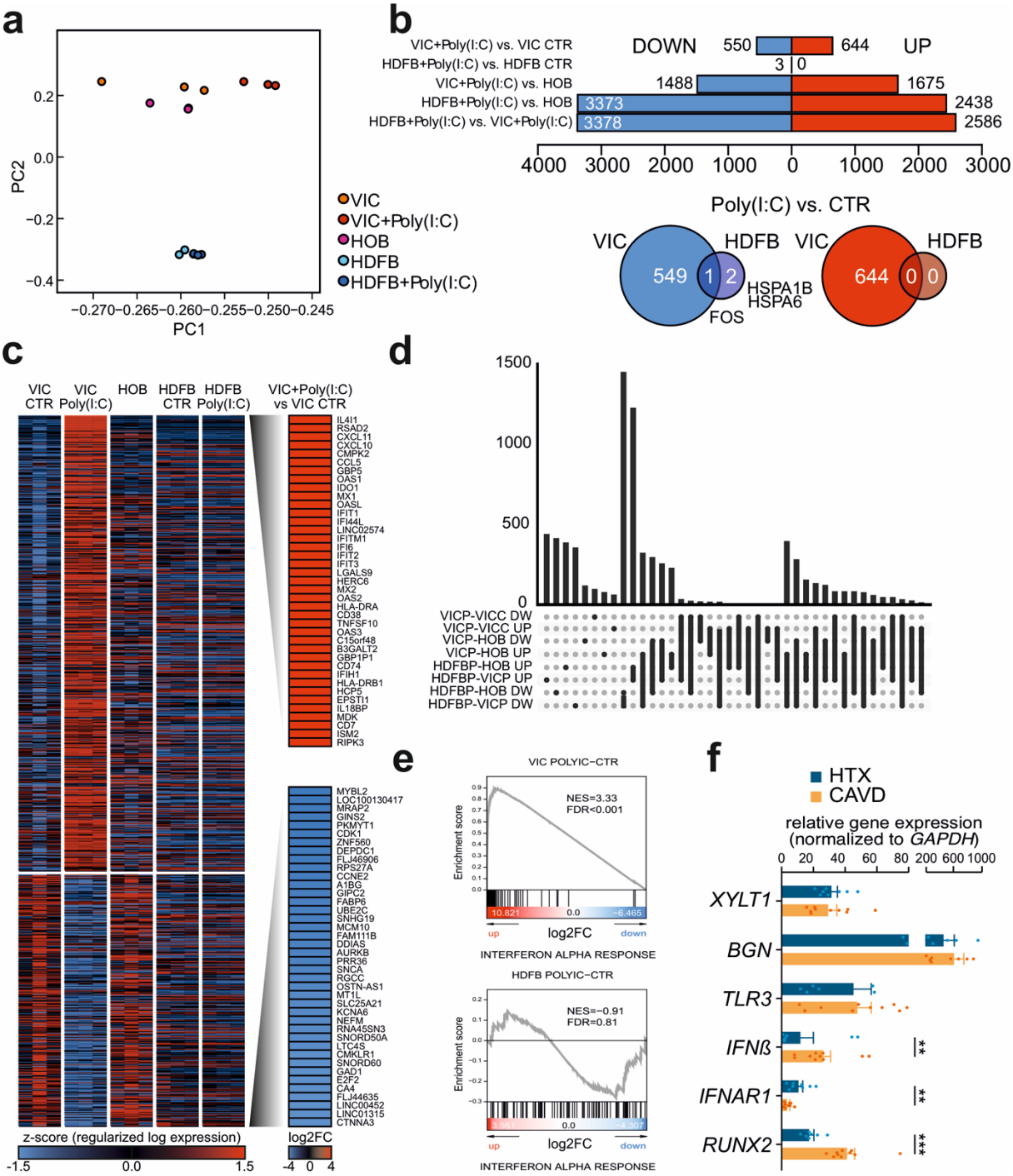

Figure S8: RNA sequencing comparing expression profiles of hVICs, human dermal fibroblasts and human osteoblasts.

For the analysis, hVICs and human dermal fibroblasts (hdFB) were treated with Poly(I:C) (20 µl/ml) for 72 h. Treated samples were compared with untreated controls and human osteoblasts (determinations in triplicate).

(a) Principal component analysis of the samples analyzed.

(b) Comparison of the genes up- or downregulated between all groups and intersection of the treated and untreated hVICs and hdFB.

(c) Heat map of all groups of genes displaying at least four-fold differential expression (red = upregulated, blue = downregulated, black = not regulated).

(d) Plot of the intersections of genes between the indicated groups.

(e) Gene set enrichment for treated hVICs versus untreated hVICs and treated hdFB versus untreated hdFB.

(f) Gene expression levels of BGN-TLR3-IFNAR1 axis in human aortic valve specimens from CAVD patients and healthy controls; *n*=10. Data are presented as mean ± SEM. Statistical comparisons. Two-tailed unpaired *t*-tests: ***P*<0.01, ****P*<0.001.

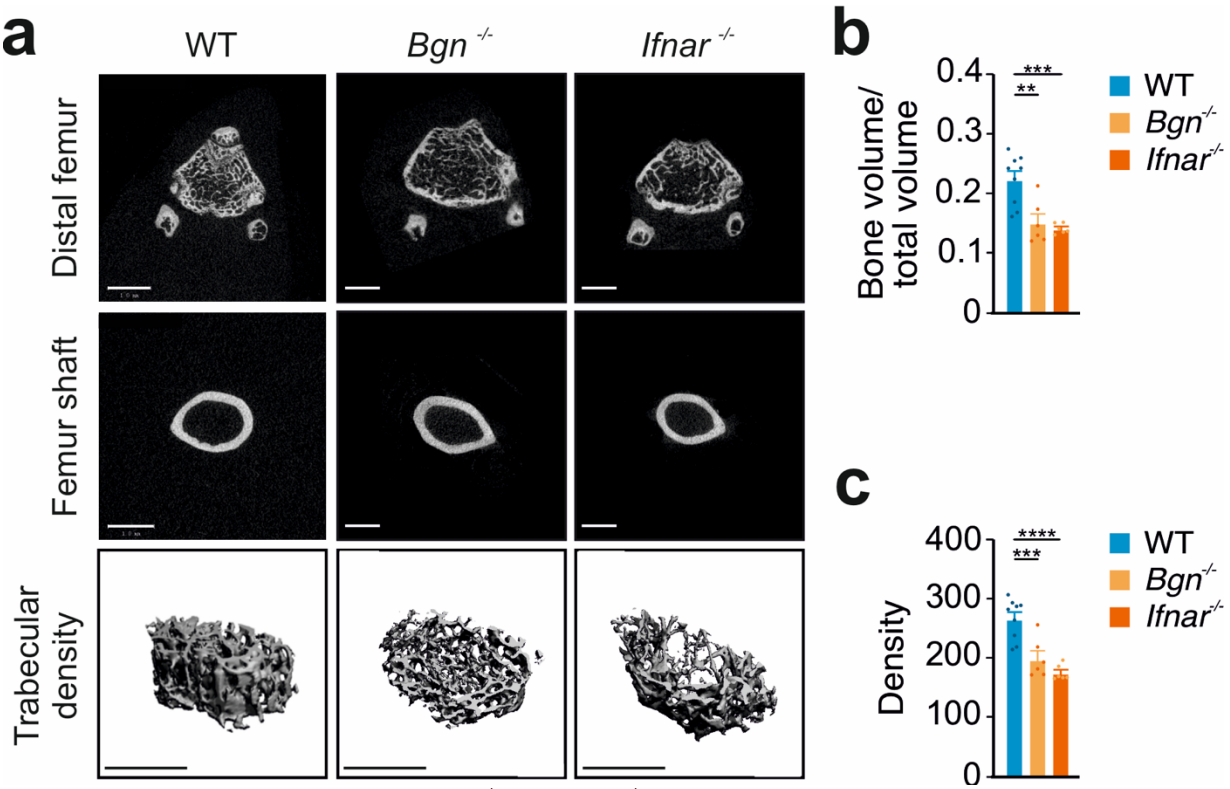

Figure S9: Osteoporotic phenotype in *Bgn*$^{-/-}$ and *Ifnar1*$^{-/-}$ mice.

(a) Femora from 12-week-old wild-type, *Bgn*$^{-/-}$ and *Ifnar1*$^{-/-}$ mice (*n*=6-9 femora) subjected to morphological analysis by micro-CT for:

(b) Bone volume, and

(c) Bone density.

All data are presented as the mean ± SEM. Statistical comparisons: One-way ANOVA with Dunnett post hoc tests: ***P*<0.01, ****P*<0.001, *****P*<0.0001,

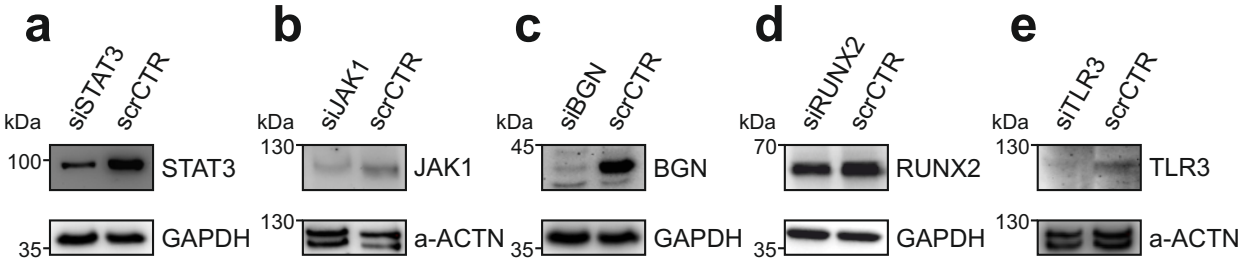

Figure S10: Validation of the specificity and linearity of antibodies.

Immunoblots of human dermal fibroblasts transfected with scr RNA or **(a)** STAT3 siRNA, **(b)** JAK1 siRNA, **(c)** BGN siRNA, **(d)** RUNX2 siRNA, **(e)** TLR3 siRNA for 24 h. Detection was performed with the corresponding antibodies.

Supplemental Tables

Method	**Odds Ratio per Normalized Effect Size (95% CI)**	***p***
Inverse-Variance Weighted	1.10 (0.92, 1.32)	0.29
Penalized Weighted Median	1.14 (1.01, 1.28)	0.032
Egger	0.88 (0.37, 2.09)	0.77
Egger Intercept	N/A	0.58

Table S1: Mendelian randomization of *XYLT1* expression in the aorta for aortic stenosis.

Chromosomal Position (GRCh37)	Variant	Expression-Increasing Allele	Other Allele	Expression in Normalized Effect Size (95% CI)	Expression *p*	Aortic Stenosis Odds Ratio (95% CI)	Aortic Stenosis *p*
16:17415463	rs6416675	C	T	0.19 (0.09, 0.28)	1.3E-04	1.02 (0.98, 1.06)	0.3
16:17436344	rs12924407	T	C	0.19 (0.09, 0.28)	8.4E-05	1.02 (0.98, 1.06)	0.45
16:17437934	rs12596741	T	C	0.16 (0.07, 0.25)	6.2E-04	1.02 (0.98, 1.06)	0.37
16:17472691	rs9929482	C	T	0.17 (0.07, 0.26)	7.3E-04	1.04 (0.99, 1.08)	0.088
16:17499765	rs8054100	G	A	0.18 (0.09, 0.28)	2.1E-04	1.03 (0.99, 1.07)	0.15
16:17505274	rs6498704	G	A	0.17 (0.07, 0.26)	4.8E-04	1.03 (0.99, 1.07)	0.12

Table S2: Associations with *XYLT1* expression in the aorta and with aortic stenosis (for variants in the Mendelian randomization instrument for aortic stenosis).

XylT-I siRNA (h)	sc-61817, Lot # K2907
RUNX2 siRNA (h)	sc-37145, Lot # E1515
Biglycan siRNA (h)	sc-43633, Lot # B2806
TLR3 siRNA (h)	sc-36685, Lot # B2718
Stat3 siRNA (h)	Sc-29493, Lot # H0917

Table S3: siRNAs

Human TLR3	FW: 5'-AGGAAAGGCTAGCAGTCATCC-3'
	RV: 5'-TAACAGTGCACTTGGTGGTG-3'
Human IFNb	FW: 5´-TGAGAACCTCCTGGCTAATGTC-3'
	RV: 5´-TTTTCAGGTGCAGACTGCTC-3'
Human XYLT1	FW: 5‘-GCTGCTGATGCCTGAGAAGGT-3‘
	RV: 5‘-GACAAAGGCGATTCTGACCGG-3‘
Mouse TLR3	FW: 5'-TTGTCTTCTGCACGAACCTG-3'
	RV: 5'-CCGTTCCCAACTTTGTAGATG-3'
Human p16	FW: 5'-GAG CAG CAT GGA GCC TTV-3’
	RV: 5'-CGTAACTATTCGGTGCGTTG-3’
Human p21	FW: 5'-GACACCACTGGAGGGTGACT -3'
	RV: 5'-CAGGTCCACATGGTCTTCCT-3'
Mouse TLR1	FW: 5'-TCAAGTGTGCAGCTGATTGC -3'
	RV: 5'-TAGTGCTGACGGACACATCC-3'
Mouse TLR2	FW: 5'- CAGCTGGAGAACTCTGACCC -3'
	RV: 5'- CAAAGAGCCTGAAGTGGGAG-3'
Mouse TLR3	FW: 5'- CCTCCAACTGTCTACCAGTTCC -3'
	RV: 5'- GCCTGGCTAAGTTATTGTGC-3'
Mouse TLR4	FW: 5'- CAACATCATCCAGGAAGGC -3'
	RV: 5'- GAAGGCGATACAATTCCACC-3'
Mouse TLR5	FW: 5'- AGCATTCTCATCGTGGTGG -3'
	RV: 5'- AATGGTTGCTATGGTTCGC-3'
Mouse TLR6	FW: 5'- TGGATGTCTCACACAATCGG -3'
	RV: 5'- GCAGCTTAGATGCAAGTGAGC-3'
Mouse TLR7	FW: 5'- TTCCTTCCGTAGGCTGAACC -3'
	RV: 5'- GTAAGCTGGATGGCAGATCC-3'

Mouse TLR8	FW: 5'- TCTACTTGGCCTTGCAGAGG -3'
	RV: 5'- ATGGCAGAGTCGTGACTTCC-3'
Mouse TLR9	FW: 5'- CAAGAACCTGGTGTCACTGC -3'
	RV: 5'- TGCGATTGTCTGACAAGTCC-3'
Mouse TLR11	FW: 5'- TCCTTCCTCTGATTAGCTGTCCTAA -3'
	RV: 5'- TCCACATAATTTCCACCAACAAGT-3'
Mouse TLR12	FW: 5'- GCCGCCATTCCAAGCTATC-3'
	RV: 5'- CTCCACAGTCCGAGGTACAACTT-3'
Mouse TLR13	FW: 5'- ATGGCACAAAACGGAGAAGAA-3'
	RV: 5'- CTTTGTATACCCATGCCTCATCAG-3'

Table S4: Primer sequences

TLR3	Cell Signaling Technologies, Danvers, MA; #6961
TRIF	Cell Signaling Technologies, Danvers, MA; #4596
TRAF6	Abcam, Cambridge, UK; ab137452
IRF3	Cell Signaling Technologies, Danvers, MA; #4302
pIRF3	Cell Signaling Technologies, Danvers, MA; #29047
IFNAR1	GeneTex, #N1N3
JAK1	Cell Signaling Technologies, Danvers, MA; #3332
pJAK1	Cell Signaling Technologies, Danvers, MA; #3331
STAT3	Cell Signaling Technologies, Danvers, MA; #9132
pSTAT3	Cell Signaling Technologies, Danvers, MA; #9145
RUNX2	Abcam, Cambridge, UK; ab23981
GAPDH (6C5)	Invitrogen, Carlsbad, CA; #AM4300
TBP	Cell Signaling Technologies, Danvers, MA; #8515
Actin	Sigma, St. Louis, MO; A2066
XYLT1	Novusbio, #NBP1-91245
BGN	R&D Systems, Minneapolis, #AF2667

Table S5: Antibodies used for western blot analysis

TLR3	abcam, Cambridge, UK; ab62566
RUNX2	abcam, Cambridge, UK; ab23981
TLR3	Cell Signaling, Danvers, US; D10F10
BGN	R&D, Minneapolis, US; AF2667

Table S6: Antibodies used for immunofluorescence staining